

INVESTIGATION OF BALL JOINTS UNDER STATIC AND DYNAMIC LOADS

G-D LEGUET^{1,2} *, *J-F ROCHE*¹, *M. A. HAMDI*², *M. RACHIK*²

¹*Zodiac Aero Duct Systems,*

5 rue des ateliers, 60200 Compiègne, FRANCE

²*Laboratoire Roberval, Université Technologique de Compiègne,*

60200 Compiègne, FRANCE

* *Email : GuillaumeDavid.Leguet@zodiac aerospace.com*

Abstract

The paper presents comparison between numerical and experimental results of static momentum stiffness of ball joint used in pneumatic aero-ducts. Through a static numerical analysis, a parametric study of the ball joint stiffness is conducted and then compared to the results of standard measurement campaign defined by Zodiac Aero Duct Systems. The dynamic behavior of the ball joint is then investigated through an experimental campaign allowing the measurement of the dynamic stiffness of the ball joint at different level of excitations and relative angle offsets.

1. Introduction

Zodiac Aero Duct System (ZADS) designs pneumatic duct systems under pressure mounted on aircraft engines, whose must withstand severe thermal and vibration environments. The air inside the ducts is extracted at high temperature (400 to 700 °C) and high pressure (5 to 30 bars) from motor compressors and then distributed through valves to the airplane to ensure defrosting of the wings, pressurization of the cab and engine starting aid (Figure 1a). Initially made up of rigid ducts (Figure 1b), the pneumatic ducts integrate flexible elements, referred as "ball joints" (Figure 1c) to reduce the mass system, to balance thermal dilatation and mechanical displacement, and provide damping.

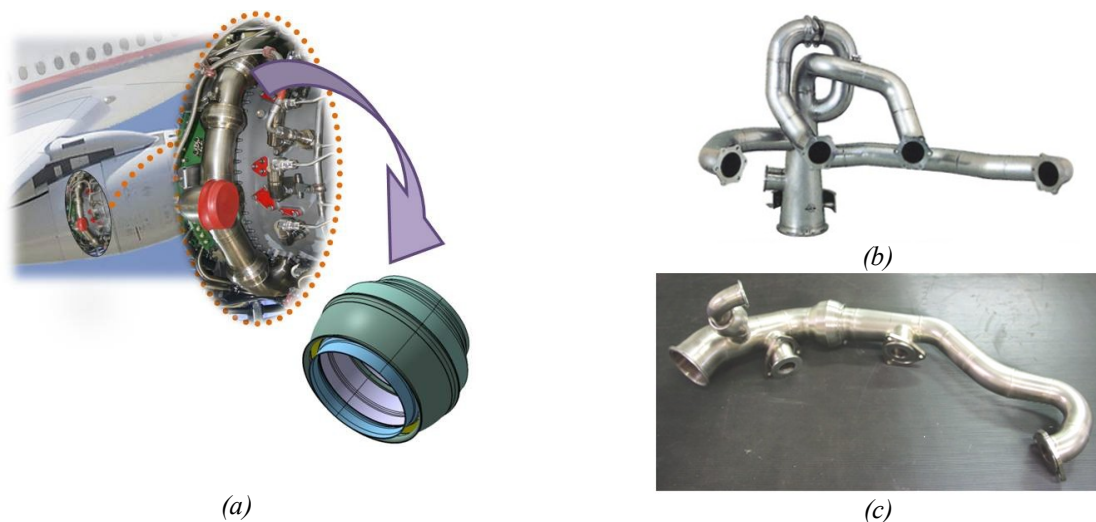


Figure 1: Ball joint in ZADS pneumatic duct systems

Vibration tests on pneumatic ducts have exhibited nonlinear behaviors depending on the excitation amplitude levels. Those nonlinear phenomena might mainly be attributed to the ball joints. The ball joint is a flexible element composed of several components (Figure 2). Its design induces a nonlinear behavior by the presence of contact, dry friction and geometric nonlinearity.

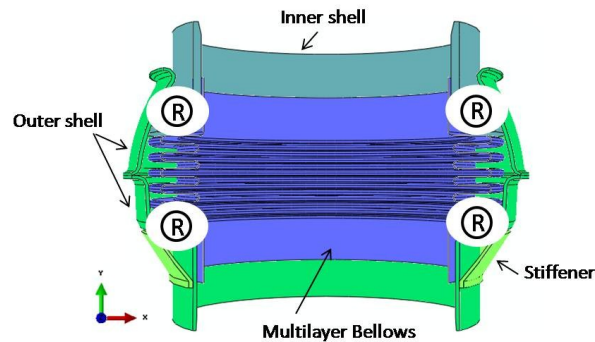


Figure 2 : Ball joint definition

Ball joints aim at ensuring the connection between ducts. The arrangement of the various elements constituting the articulation allows the rotation center of the system to coincide with the center of gravity G of the multilayer bellows (Figure 3a), allowing very good fatigue endurance in bending. Under loading, the bellows induce an angular displacement of the inner shell relative to the outer shell. The friction in the contact area is induced by a graphic bearing. Kinematically the ball joint is equivalent to a spherical joint (Figure 3b), this element allows a relative angular displacement around the x and z axes.

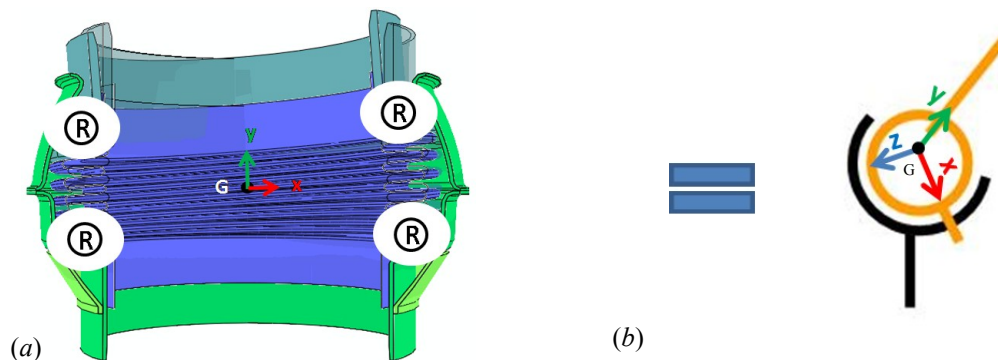


Figure 3: Ball joint cinematic

Compliance tests are performed on ZADS pneumatic ducts according to the aeronautical standards. In regards to the aeronautical standards vibration tests [1], [2] (RTCA DO 160 or MIL-STD-810), the pneumatic ducts therefore the ball joints are submitted to static loads. Those static loads are induced by pressure, temperature and misalignment between the tooling depending on the qualification test procedure definition. Under static loading the ball joint can undergo a relative angular displacement offset, despite being initially aligned with its axis of symmetry. This induces an asymmetry of the system. At a relative angle displacement offset the structure is solicited by dynamic loads which could be random or determinist. Static and dynamic experimental tests have been carried out and experimental results are compared to numerical results using Finite Element Models of the ball joint.

2. Static step

2.1 Experimental setup

A quasi static test bench has been installed at ZADS to measure the ball joints moment (Figure 4a and 4b). One end of the ball joint is grounded to a suitable mounting point, leaving the opposite end free. A level arm is attached to the free end of the ball joint to enable deflection. An angular displacement is applied by means of a hydraulic double acting jack coupled with a spherical joint.

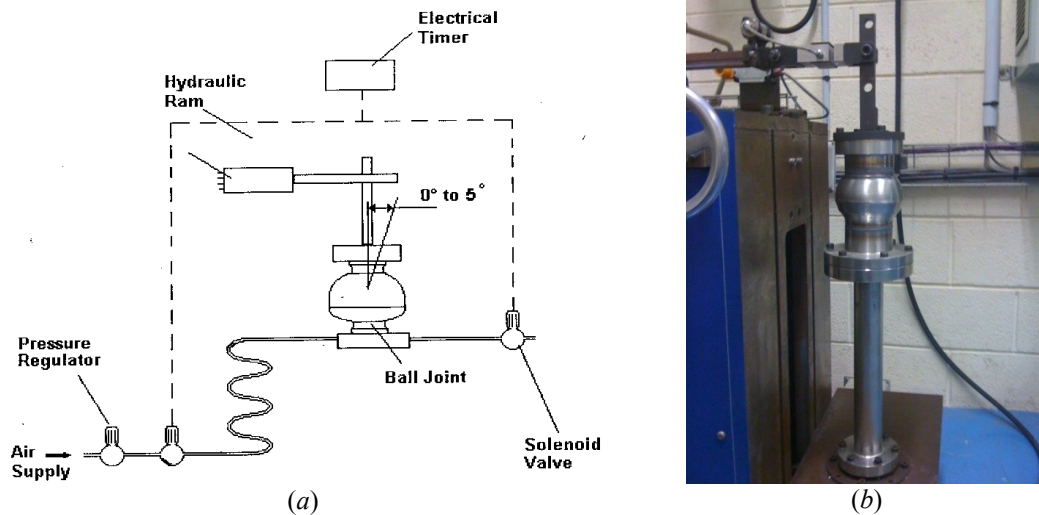


Figure 4: Static experimental setup

The ball joint moment is then determined by the relation

$$M = F_T \cdot R \quad (1)$$

Where F_T is the tangential force measured by a dynamometer and R the lever arm from the rotation center G to the force application point.

The moment M has been investigated on a ball joint of 102 mm nominal diameter with a relative angle up to 7 degrees. The ball joint multilayer bellows is manufactured from inconel 625 using hydroforming process. The inner and outer shells are manufactured from austenitic stainless steel using stamping or spinning process. For an optimization of the moment a graphic bearing is used as a solid lubricant. The test is carried out at room temperature, the ball joint air pressure, is controlled by an analogue pressure gauge, and is adjusted to 5 bar. The force is recorded at each degree from 1 to 3°. The relative angle was studied up to 3° due to the test bench limitation. The hydraulic double acting jack coupled with a spherical joint cannot undergo larger angle without adding some errors in the measured moment. Table 1 gives the values of the Momentum values at 3 angle positions.

Table 1: Bending moment

	M(θ) experimental			unity
M	73.8	75.8	77.6	N.m
θ	1	2	3	degrees

2.2 Numerical simulation methodology

A Finite Element Model (FEM) of the ball joint was developed in order to determine the moment by numerical simulations. The geometry is first acquired in CATpart format. In the assembly model, a disk is added on the top of the inner shell, so as to add a bottom pressure.

A hypothesis was made on the bellows thickness modeling. The bellows is composed of three layers using hydroforming process. Each layer is 0.15 mm thick. The standard of the expansion joint manufacturers association (EJMA) [1], gives the stiffness calculation formula of multi-layer bellows. A common approach consists of using an equivalent mono-layer bellows thickness which gives the same EJMA axial stiffness of the multi-layer bellows. Based on the bellows geometry and number of layers, the equivalent thickness value is 0.22 mm (EJMA).

A finite element analysis were conducted using ABAQUS software to calculate the ball joint moment. ABAQUS element library includes a wide range of element types. Depending on their geometries, specifics elements were assigned to the different ball joint parts. Shell elements type S4R (Shell, 4-node, Reduced integration) were used for

the equivalent stiffness bellows. Solid elements type C3D8R (Continuum, 3D, 8-node, Reduced integration) were used for the graphic bearing and continuum shell CS8R (Continuum Shell, 8-node, Reduced integration) for the inner and outer shells. Continuum shell was used instead of shell or solid elements. Solid elements would imply at least 5 elements in the thickness while continuum shell elements need only one element and are more accurate for contact modeling than conventional shells. The upper disk is modeled as rigid solid. The material inconel 625 is assigned to the bellows, austenitic (AISI 321) stainless for the inner and outer shells and a special graphic (JP 1932) is used for the bearing graphic. The material is modeled as linear, homogeneous and isotropic.

For each of the two ends, two different types of boundary conditions were used to simulate the experimental test. Experimentally, one end of the ball joint is connected to a thick duct. A hypothesis was made that the thick duct was not deformed under loading. Numerically the edge is clamped by imposing no displacement. At the second end of the ball joint a displacement is imposed at a reference point kinematically coupled with the edge of the inner shell (Figure 5).

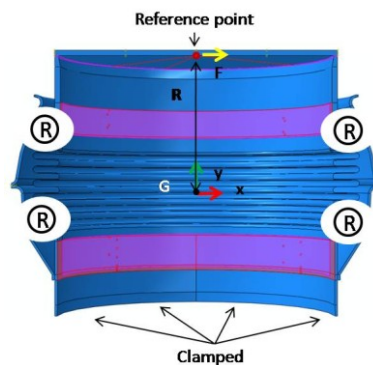


Figure 5: Boundary conditions and kinematic / tie coupling

The computation is split in four static general steps. In the first step the contact between the elements is established. The type of contact used is "Surface-to-surface contact" with a finite sliding formulation. At the initial step there is some penetration of the slave surface into the master surface due to the oversize bellows dimension. An automatic shrink fit on overclosure adjustment option is used to reposition the slave part which induces a bellows compression. The normal behavior contact used for "Pressure-Overclosure" is "Hard"Contact, while "Default" is used for "Constraint enforcement method. The tangential behavior uses the penalty formulation and the friction coefficient for the first step is considered null. The friction coefficient μ is then changed in a second step from 0 up to 0.2. In a third step the ball joint is pressurized. "Nlgeom" is set on for all the steps in order to take into account the bellows geometry nonlinearities. For the last step a displacement is imposed at a reference point kinematically coupled with the edge of the inner shell. The displacement induces a relative angular displacement of the ball joint inner shell up to 5 degrees.

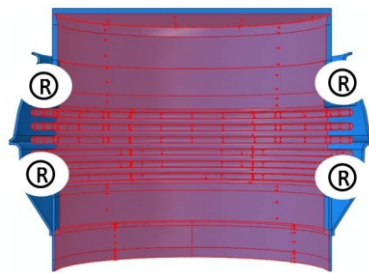


Figure 6 : Pressure load ball joint

2.3 Comparison of Experimental-Numerical results

In ABAQUS, a coulomb friction law's was used to take into account the friction induced by the graphic bearing. Normal and tangential forces are linked by the friction coefficient. Equation (1) can be rewritten as following

$$M = \mu \cdot F_N \cdot R \quad (2)$$

where μ is the dry friction coefficient, F_N the normal force and R the lever arm. From equation 2, the moment depends on the dry friction coefficient μ and tangential force F_N since the lever arm R is a constant. The normal force hinges on the bellows multilayer stiffness and so on the applied pressure.

Based on the assumptions from ZADS experimental ball joint results, the moment is represented by a rheological model (Figure 7a and 7b). The model is characterized by a sliding resistance pad in parallel to a spring. The moment is then expressed as

$$M = K\theta + M_y \quad (3)$$

where M is the ball joint bending moment, θ the relative angle, M_y is the sliding threshold and K is the ball joint stiffness. The relative angle θ is determined from the imposed displacement U by the relation

$$\theta = \tan^{-1}\left(\frac{U}{R}\right) \quad (4)$$

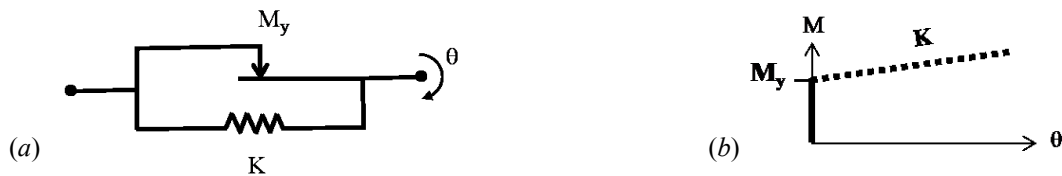


Figure 7 : Rheological model of the ball joint moment

In equations 2 and 3, the ball joint moment is expressed by its friction coefficient μ and normal force F_N or its sliding threshold M_y and stiffness K . The second approach is investigated. A parametric study is carried out on the friction coefficient μ , the equivalent bellows thickness δ and the pressure p in order to evaluate their influence on the sliding threshold M_y and the ball joint stiffness K .

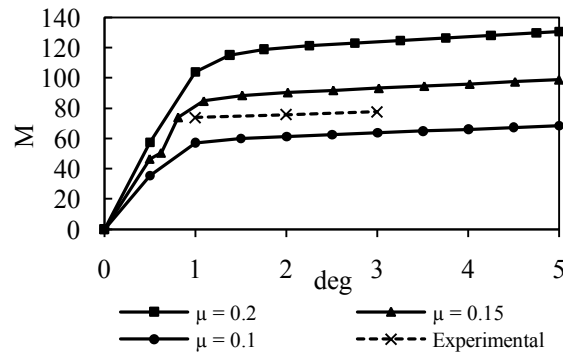
Some assumptions are made regarding the range of the ball joint parameters. From previous studies, the friction coefficient $\mu \in [0.1 ; 0.2]$. The equivalent bellows thickness value is 0.22 mm (EJMA). The thickness is studied in the range $\delta \in [0.15 ; 0.3]$ mm where 0.15 mm is the thickness of one layer. During the test the pressure is controlled by analogue pressure gauge. In order to take into account measurement uncertainty $p \in [4 ; 6]$ bar.

The first parameter studied is the friction coefficient μ . The pressure parameter is fixed at $p_0 = 5$ bar and the equivalent bellows thickness at $\delta_0 = 0.22$ mm. Table 2 shows values of the friction coefficient .

Table 2 : Friction coefficient values

Friction coefficient (μ)						unity
0.10	0.11	0.13	0.15	0.18	0.2	
^a $p_0 = 5$ bar and $\delta_0 = 0.22$ mm						

The moment is calculated for each value of the friction coefficient. Figure 8 presents the results for three values of the friction coefficient μ : 0.1, 0.15 and 0.2 .

Figure 8: Moment as a function of μ

Initially the ball joint is at a stick state. In ABAQUS, the first size increment can be adjusted automatically or defined by the user. Figure 10 shows the moment at $\mu = 0.1$ calculated for two different initial increments (0.1, 0.01). To reduce the computation time, the first increment is set on automatically in ABAQUS.

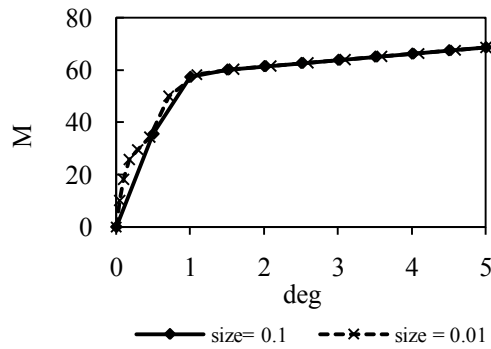
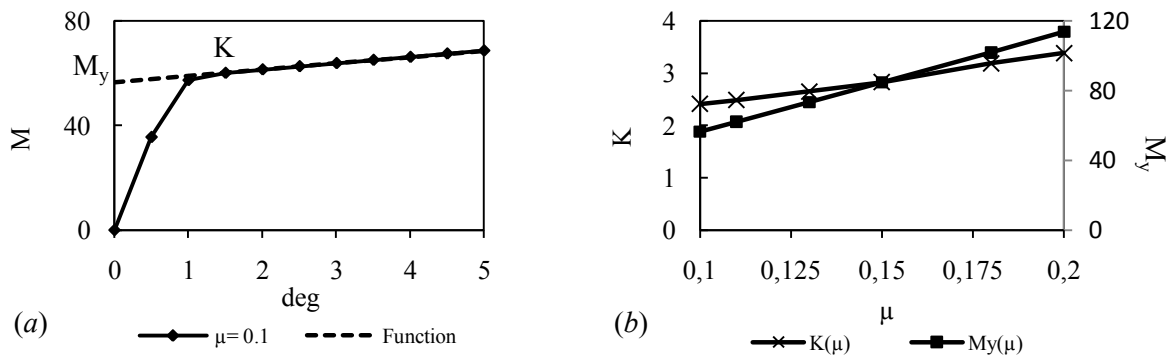


Figure 9: Size increment effect on the slope

The stiffness K and the sliding threshold M_y obtained by curve fitting was determined for each value of the friction coefficient μ as shown in Figure 10a. Figure 10b shows the dependency of K and M_y as function of μ .

Figure 10 : (a) Determination of K and M_y by curve fitting the numerical moment M , (b) $K(\mu)$ and $M_y(\mu)$

A sensitivity study of K and M_y function of μ is carried out using the relations

$$\Delta\mu_K = \frac{\partial K}{\partial \mu}(\mu, p_0, \delta_0) \quad (5)$$

where $\Delta\mu_K$ is the slope rate of the ball joint stiffness K regarding the friction coefficient μ , $p_0 = 5$ bar and $\delta_0 = 022$ mm.

$$\Delta\mu_{M_y} = \frac{\partial M_y}{\partial \mu}(\mu, p_0, \delta_0) \quad (6)$$

where $\Delta\mu_{M_y}$ is the slope rate of the sliding threshold M_y regarding the friction coefficient μ at $p_0 = 5$ bar and $\delta_0 = 0.22$ mm.

The same procedure is carried out for the pressure (p) and the equivalent bellows thickness (δ) Table 3 and 4. The moment are calculated, then K and M_y are determined function of p and δ . Finally a sensibility study is carried out for each parameter.

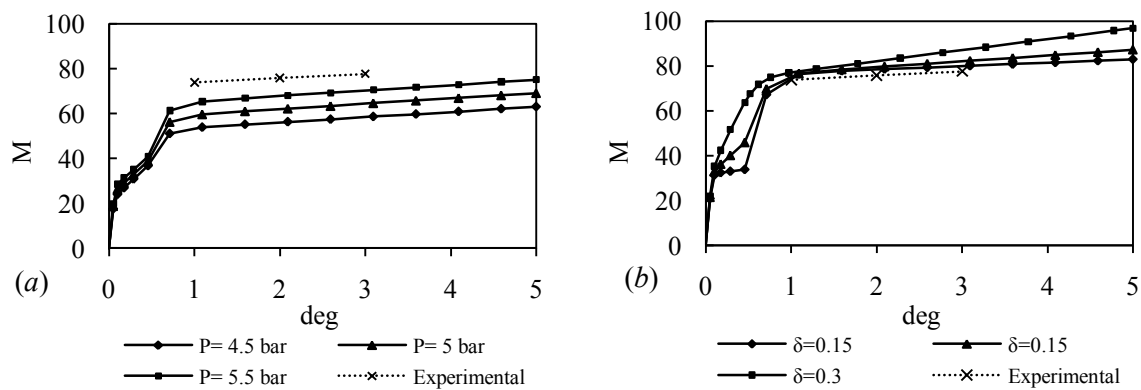
Table 3 : Parameter p

Pressure (p) ^a						unity
4	4.5	5	5.5	6		bar
^a $\mu_0 = 0.13$ and $\delta_0 = 0.22$ mm						

Table 4 : Parameter δ

Equivalent thickness bellows (δ) ^a					unity
0.15	0.19	0.22	0.26	0.3	mm
^a $\mu_0 = 0.13$ and $p_0 = 5$ bar					

Figures 11 (a) and (b) show the Momentum results relative to the pressure (p) and thickness (δ) parameters.

Figure 11: Moment as a function of (a) the pressure p , (b) the equivalent bellows thickness δ , for $\mu = 0.13$

The results obtained from the sensibility study are presented Table 5 and 6.

Table 5 : Sensibility K results

	K	unity
$\Delta\mu_K$	0.73	
Δp_K	0.99	Nm/bar
$\Delta\delta_K$	$4.26 \delta + 1.25^a$	Nm/mm

$$^a K(\delta) = 2.18 \text{ for } \delta = 0.22 \text{ mm}$$

Table 6 : Sensibility M_y results

	M_y	unity
$\Delta\mu_{M_y}$	59.13	
Δp_{M_y}	57.13	Nm/bar
$\Delta\delta_{M_y}$	-3.14	Nm/mm

The ball joint stiffness K depends on the three parameters but mostly on the equivalent bellows stiffness (Table 5). As illustrated in Table 6, the effect of the equivalent bellows stiffness δ on the sliding threshold M_y can be neglected. The sliding threshold M_y is relying only on the friction coefficient μ and the pressure p (Table 6). The pressure was measured during the experimental campaign by an analogue pressure gauge.

By minimizing the difference between numerical and experimental sliding threshold, the value of the friction coefficient μ can be determined for a fixed pressure since the bellows stiffness remains not effected. Then knowing μ and p the equivalent bellows stiffness can be evaluated.

To match the experimental sliding threshold $M_{y\ exp}$, and assuming some uncertainty on the measured pressure, the friction coefficient is determined belonging to the range $\mu \in [0.11 ; 0.13]$ for $p \in [4.5 ; 5.5]$ bar. In the friction coefficient and pressure ranges, the equivalent stiffness is evaluated at $\delta \in [0.18 ; 0.2]$ mm. Figure 12 shows the overlay of the experimental and the numerical moment for $\mu = 0.125$, $p = 5$ bar and $\delta = 0.19$ mm.

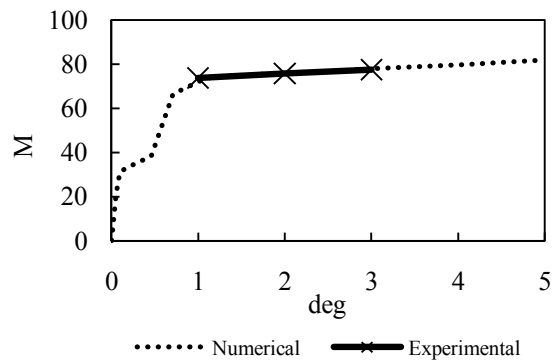


Figure 12 : Comparison experimental and numerical moment with $\mu = 0.125$, $p = 5$ bar and $\delta = 0.19$ mm.

Several remarks can be done regarding the parametric study on the ball joint. The equivalent bellows stiffness base on the axial stiffness (EJMA) seems to overestimate the bending stiffness of the ball joint bellows. From this approach, the friction coefficient can be determined, and then be used for nonlinear dynamic simulation. Due to a lack of information and uncertainty regarding the experimental measurement some tests are scheduled in order to check the bellows stiffness and friction coefficient values.

3. Dynamic step

The ball joints in the static and dynamic part are different. The ball joint in the dynamic part is different by its number of bellows layers, nominal diameter and material proprieties of the inner and outer shells.

3.1 Experimental setup

A test bench has been set up in order to investigate the dynamic behavior of the ball joint (Figure 13). A specific tooling has been developed to allow pressurization and attachment of the shaker on the ball joint. The tooling has been dimensioned so that its dynamic behavior does not interfere with the ball joint in the frequency band (10-1800Hz).

The dynamic behavior has been investigated on a ball joint of 63.5 mm nominal diameter with a relative angle up to 7 degrees. The ball joint is a five multilayer bellows manufactured from inconel 625 using hydroforming process. Each layer is 0.15mm thick. The inner and outer shells are manufactured from inconel 625 using stamping or spinning process. For an optimization of the moment a graphic bearing is used as a solid lubricant. The test is carried out at room temperature. At this stage of the ball joint study, the test has not been carried out with pressure.

The ball joint is clamped on an steel block at one end and excited by Bruel & Kjaer Exciter Type 4824 suspended in free-free condition on the other side. A head impedance Type 8001 is placed between the stinger and the ball joint in order to measure simultaneous force and acceleration at the driving point. Two accelerometers (PCB 356A01 Triaxial accelerometer) are used on the top of the inner and the middle of the outer shells respectively (Figure 15a).



Figure 13: Dynamic test bench

Under static loading the ball joint can undergo a relative angular displacement offset, despite being initially aligned with its axis of symmetry. This induces an asymmetry of the system which might change its dynamic behavior. In order to take into account a possible asymmetry of the ball joint, the dynamic behavior of the articulation has been studied for two different relative angular displacements on the z axis (Figure 15a). No relative angular displacement is applied on the x axis. The angular offset is checked by a magnetic inclinometer in both direction x and z. For each configuration the shaker position is adjusted in order to keep the excitation normal to the ball joint. The two configurations are shown in Figure 15b and 15c. The relative angular is accentuated on Figure 15c to make the comprehension easier.

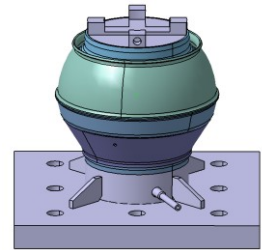


Figure 14 : Tooling

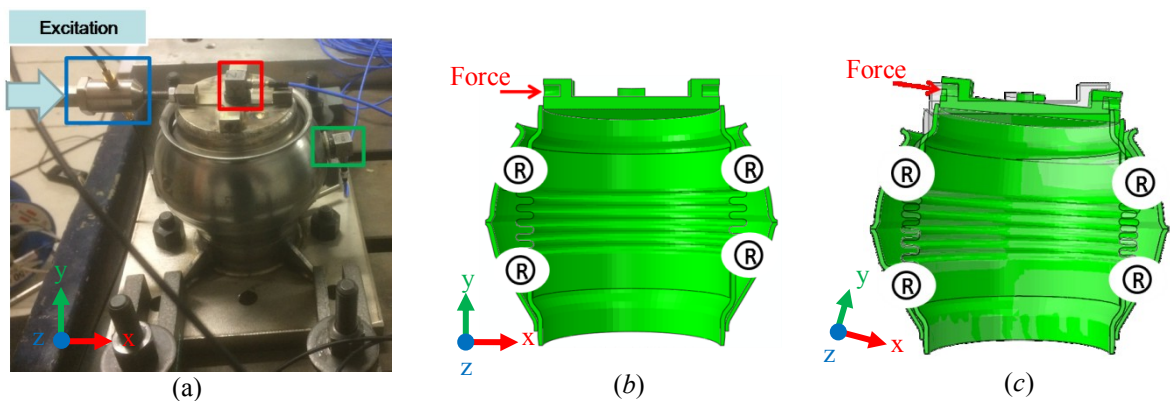


Figure 15 : (a) view bench test with reference coordinate and positions of the sensors, (b) configuration 1: initially centered, (c) configuration 2 with a relative angle offset of 0.95 degree

The relative angles have been controlled with a magnetic inclinometer. Configuration 1 were 0° in z and 0° in x axis; and configuration 2 were 0.95° in z and 0° in x axis (Figure 16a and b).

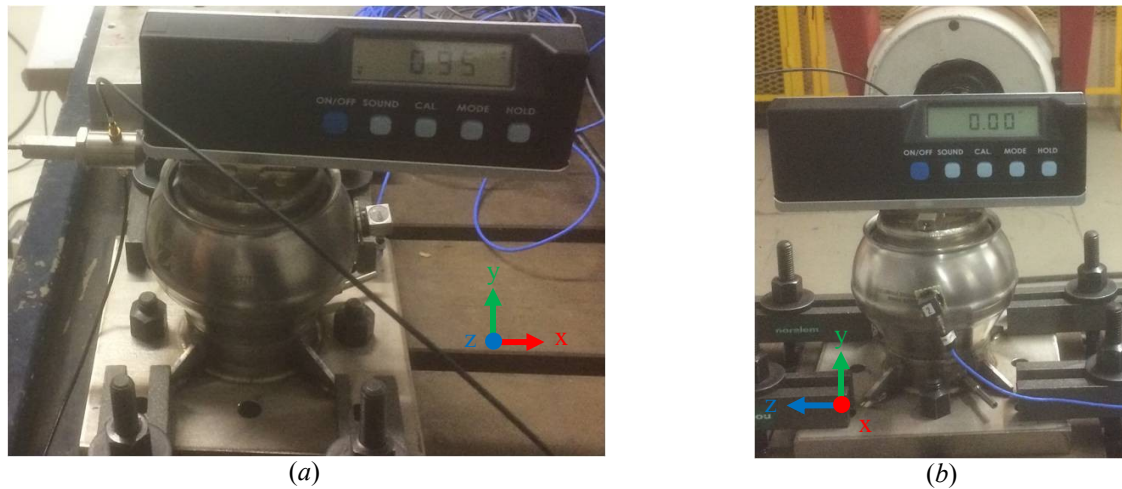


Figure 16 : Configurations 2 control relative angle, (a) z axis, (b) x axis

Due to the ball joint design, nonlinearities are expected. There are two common approaches to experimentally determine the frequency response curves of a nonlinear structure, namely the FRFs at constant force level or at a constant response level [3]–[6]. Keeping the force level constant allows to highlight the nonlinearities while keeping the response constant generates an effectively quasi linear structural behavior around the main resonances at the different input levels. The control of the force or the response was carried out by SIEMENS LMS TESTLAB 15A MIM Sweep & Stepped Sine Testing System. The signal used is a sinus step to step. Preliminary tests have been carried out with force control in order to get used with the software and the structure. A saw tooth effect has been observed on the input signal force when using level control. Initially set up on default, the LMS control parameters have been modified according to [7] in order to reduce the saw tooth phenomenon.

Five main parameters affects the measurement:

- The first parameter is the Confidence in Measured System FRF (CMS). Before each test, a white noise signal is passed to the system. The control algorithm uses this test as a reference and assumes that the system will be unchanged for all frequencies and output amplitudes. Set to low, the algorithm does a quasi-loop control in which it uses the previous measurement as a starting point for the controlling. In the case of nonlinear systems, the Frequency Response Function (FRF) depends on the excitation level.
- The second parameter is the Error Correction Factor (ECF) which determines how much the algorithm corrects the divergence from the control band in one frequency step. When the factor is set to low, the algorithm may not correct the divergence from the control level enough in a step. For the study the ECF is set at 60%.
- The third parameter is the Number of Delay Cycles (NDC) which allows to choose the number of cycles that the acquisition system must wait before starting the measurement. A large number ensures that only the stationary part of the measurement is retained. For the study, the NDC is fixed at 30 cycles.
- The fourth parameter is the Number of Hold Cycle (NHC). The NHC is used to select the number of periods involved in the Fourier Transform. A large number of periods can reduce aliasing effects however can increase the time test.
- The fifth and last parameter is the Step Size parameter which defined the increment size. A large increment may result in a sudden change on the measured force or response. This change makes the control more difficult. Ref [7] this parameter is fixed at 0.05Hz.

Tableau 7 : Control parameters used for force and displacement control levels

Fixed Control Parameters			
CMS	ECF	NDC	NHC
Low	60%	30	40

The ball joint for both configurations (Figure 15b and 15c) is submitted by a sinus step by step at 0.5N force level control in the frequency band (50-2000Hz).

Figure 17 shows the FRFs measured for the two configurations at 0.5N force level. Regarding the two configurations, the predominant modes are around (1000-1250Hz). The asymmetry induced by a relative angle of 0.95° configuration 2, has shifted the resonance frequency of the main mode to the left with a lower amplitude.

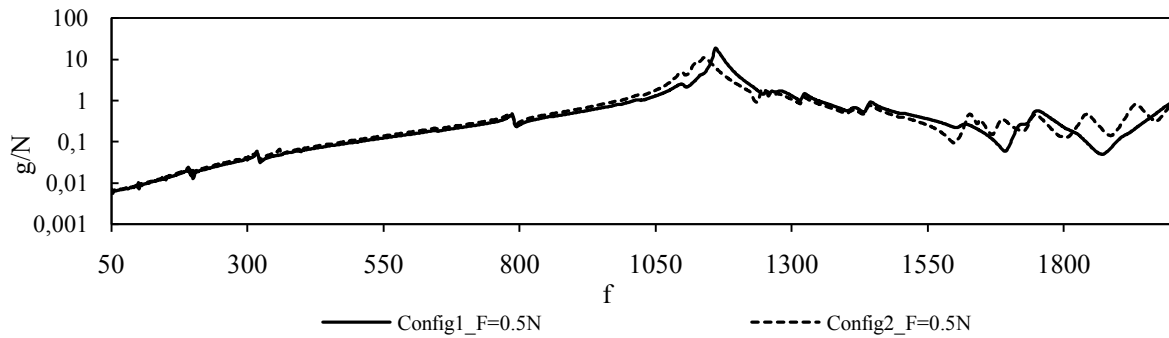


Figure 17 : FRFs of configuration 1 and 2 over the entire frequency range (50-2000Hz)

A second measurement is conducted for both configurations at 1N force level control (Figure 18).

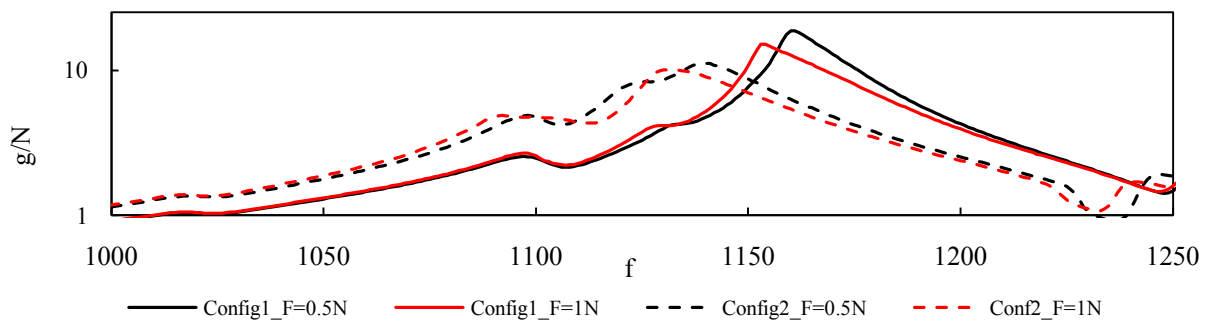


Figure 18 : FRFs of configuration 1 and 2 around the main frequency resonant for two levels of force excitation 0.5 N and 1N

The change from 0.5N to 1N of the force excitation level induced a shift to the left and an amplitude decrease of the Frequency Responses Function (FRF) for both configurations. In order to cover a large frequency band (50-2000 Hz) within a reasonable test time, the Step Size has been fixed to 1Hz.

A test around the main mode in configuration 1 with a smaller Step Size set of 0.05Hz is conducted in the frequency band (1120-1180 Hz). The results corresponding to the two Step Size are compared through their auto spectrum (N^2) (Figure 19a) and FRF (Figure 19b). The control algorithm is supposed to keep the force constant over the whole frequency band. As illustrated in Figure 19, this is achieved for the smallest frequency step of 0.05Hz. A largest Step Size of 1 Hz leads to erroneous force control (Figure 19a) and significantly affect the nonlinearities shape (Figure 19b).

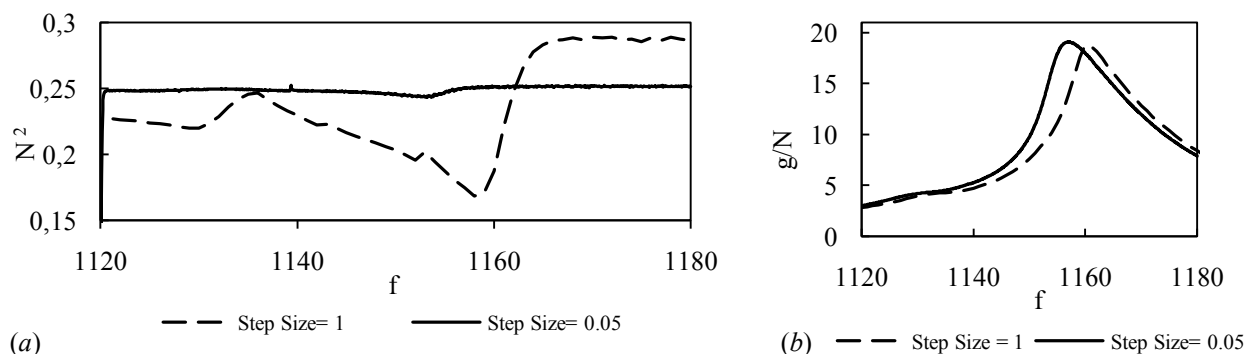


Figure 19 : Effect of the Step Size on the constant force control level

A local study in the frequency range (1120-1180Hz) in configuration 1 (Figure 15b) is then carried out with a frequency step size of 0.05 Hz in order to analyze more precisely the ball joint nonlinearities. Four level of excitation 0.1N, 0.5N, 1N and 2N, using force control, are applied at the driving point.

Figure 20a shows the frequency and amplitude dependency of the system revealing nonlinearities with respect to the excitation levels. The resonant frequency shifts to the left, indicating the stiffness softening characteristics of contact interface. The measured amplitude (frequency response function) reveals damping in the structure. The increase in the damping is a direct result of initiation of micro-slips in the contact interface [8]. The hysteresis phenomena is observed on the ball joint for configuration 1 (Figure 20b), with a sinus step by step from the low frequency to the high frequency (up) and on the other side (down) at 1N force level.

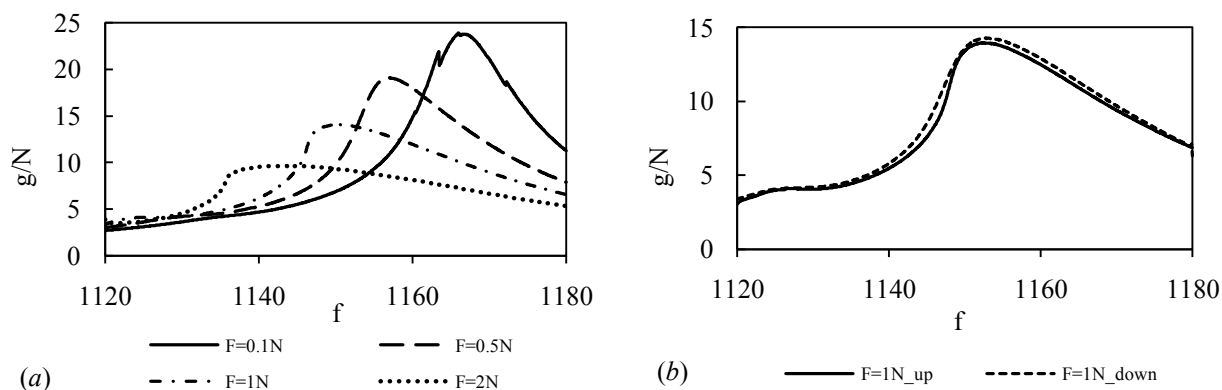


Figure 20 : Zoom at the main modes of the ball joint in the range for the configuration 1, (a) in the frequency range (1120-1180Hz), (b) hysteresis phenomena of the ball joint under step by step up and down

The second measurement campaign consisted of maintaining the response level constant. This approach enables the use of classical linear modal extraction tools. However response level control approach can only be used in a narrow frequency band around the resonance of an isolated non-linear mode. Due to its application restriction, the response level control was applied only for the configuration 1. The displacement is controlled at the driving point. Three levels have been considered: 0.0005mm, 0.001mm and 0.0015mm. The displacement of 0.0015mm corresponds at 1180 Hz to an acceleration level of 8.4g which is twice lower than the aeronautical standards [2].

The software Pulse reflex has been used to carry out the modal identification. (Figure 21b) shows the stability diagram illustrating the quasi-linear behavior of the ball joint.

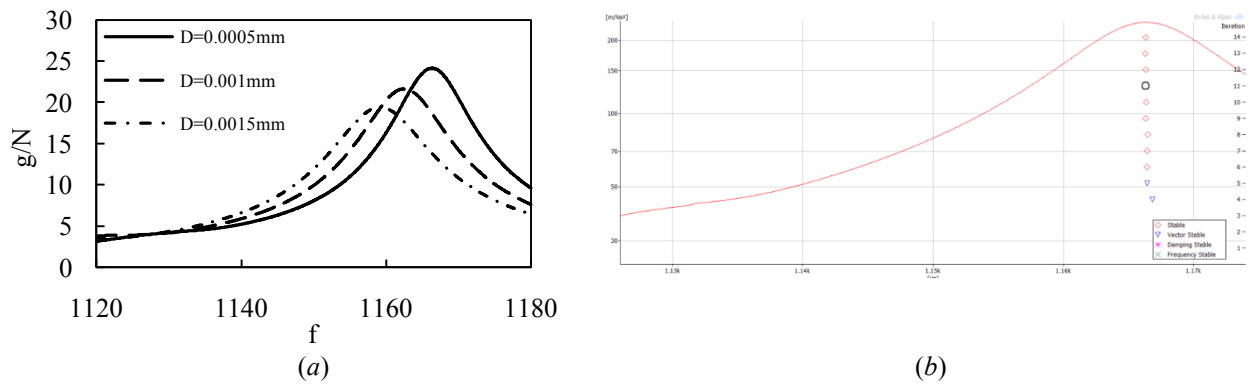


Figure 21 : FRFs in configuration 1 (a) under displacement control levels, (b) modal identification of the ball joint at the main resonance under 0.0005mm displacement control using Pulse Reflex by B&K .

Table 8: Modal identification of the ball joint main resonance for three displacement control level

Excitation Level mm	Excitation Level G max	Damped Frequency (Hz)	Modal Damping (%)
0.0005	2.75	1166.5	0.50
0.001	5.3	1162.5	0.56
0.0015	8.4	1159.3	0.61

Table 8 gives the extracted three values of damped frequencies and damping loss factors, which will be used for ball joint numerical models to be developed in near future to numerically predict the response of the ball joint.

The experimental campaign shows that the ball joint exhibits nonlinear dynamic behavior with respect to the level of excitation and that the dynamic stiffness is also highly depending on the relative angular offset.

4. CONCLUSION AND PERSPECTIVES

A Finite Element (FE) numerical static study has been conducted on a ball joint allowing the identification of the friction coefficient μ using a curve fitting between numerical results and existing experimental results conducted by Zodiac Aero Duct System. The FE static study showed that outside low values of the relative offset angle, the momentum could be considered as a quasilinear function.

A dynamic experimental campaign have been conducted on a ball joint and highlighted the nonlinear dynamic behavior of the ball joint dynamic stiffness for different relative angle offsets. The results of the experimental campaign will be completed using different pressure levels and will be used for the validation of the FE numerical results to be developed in near future to analyze the nonlinear behavior of the ball joint. The dynamic stiffness matrix of the ball joint will be integrated in the global FE model of the pneumatic duct system to predict the dynamic response of duct systems.

References

- [1] S.EJMA, INC, Standards of the expansion joint manufacturers association (EJMA). Inc. Ninth Edition.
- [2] MIL-STD 810: Environmental Engineering Considerations and Laboratory Test.
- [3] Ewins D.J. 2000. Modal Testing: Theory, Practice and Application. 2nd E. Research Studies Press, Baldock, UK.
- [4] K. Worden, G. Tomlinson. 2001. Nonlinearity in Structural Dynamics - Detection, Identification and Modelling. Institute of Physics Publishing, Bristol.
- [5] D. Göge, M. Sinapius, U. Füllekrug, M. Link. 2005. Detection and description of non-linear phenomena in experimental modal analysis via linearity plots. International Journal of Nonlinear Mechanics 40.
- [6] K. Vanhoenacker, J. Schoukens, J. Swevers, D. Vas. 2002. Summary and Comparing Overview of Techniques for the Detection of Non-Linearities. Proc. of the International Conference on Noise and Vibration Engineering ISMA 2002. Leuven, Belgium.
- [7] S. Catalfamo, S. A, & Zhu, D. 2016. Effects of Experimental Methods on the Measurements of a Nonlinear Structure. IMAC 34.
- [8] H. Ahmadian, H. Jalali, F. Pourahmadian. 2010. Nonlinear model identification of a friction contact support. Mechanical Systems and Signal Processing 24.